Gkoktsi K and Giaralis A (2020) A compressive MUSIC spectral approach for identification of closely-spaced structural natural frequencies and post-earthquake damage detection. *Probabilistic Engineering Mechanics*, accepted.

A compressive MUSIC spectral approach for identification of closely-spaced structural natural frequencies and post-earthquake damage detection

KYRIAKI GKOKTSI[1] and AGATHOKLIS GIARALIS[1]

[1]*Department of Civil Engineering, City, University of London, UK.*

E-mail: agathoklis@city.ac.uk

Abstract

Motivated by practical needs to reduce data transmission payloads in wireless sensors for vibration-based monitoring of engineering structures, this paper proposes a novel approach for identifying resonant frequencies of white-noise excited structures using acceleration measurements acquired at rates significantly below the Nyquist rate. The approach adopts the deterministic co-prime sub-Nyquist sampling scheme, originally developed to facilitate telecommunication applications, to estimate the autocorrelation function of response acceleration time-histories of low-amplitude white-noise excited structures treated as realizations of a stationary stochastic process. Next, the standard multiple signal classification (MUSIC) spectral estimator is applied to the estimated autocorrelation function enabling the identification of structural natural frequencies with high resolution by simple peak picking in the frequency domain without posing any sparsity conditions to the signals. This is achieved by processing autocorrelation estimates without undertaking any (typically computationally expensive) signal reconstruction step in the time-domain, as required by various recently proposed in the literature sub-Nyquist compressive sensing-based

approaches for structural health monitoring, while filtering out any broadband noise added during data acquisition. The accuracy and applicability of the proposed approach is first numerically assessed using computer-generated noise-corrupted acceleration time-history data obtained by a simulation-based framework examining white-noise excited structural systems with two closely-spaced modes of vibration carrying the same amount of energy, and a third isolated weakly excited vibrating mode. Further, damage detection potential of the developed method is numerically illustrated using a white-noise excited reinforced concrete 3-storey frame in a healthy and two damaged states caused by ground motions of increased intensity. The damage assessment relies on shifts in natural frequencies between the pre-earthquake and post-earthquake state. Overall, numerical results demonstrate that the considered approach can accurately identify structural resonances and detect structural damage associated with changes to natural frequencies as minor as 1% by sampling up to 78% below Nyquist rate for signal to noise ratio as low as 10dB. These results suggest that the adopted approach is robust and noise-immune while it can reduce data transmission requirements in acceleration wireless sensors for natural frequency identification and damage detection in engineering structures.

Keywords: co-prime sampling, MUSIC pseudo-spectrum, compressive sensing, spectral estimation, system identification, closely-spaced modes.

Gkoktsi K and Giaralis A (2020) A compressive MUSIC spectral approach for identification of closely-spaced structural natural frequencies and post-earthquake damage detection. *Probabilistic Engineering Mechanics*, accepted: 27/12/2019.

1 Introduction and motivation

Accurate identification of the natural frequencies of large-scale (civil) engineering structures and structural components is key to several important practical applications such as: the design verification of structural systems sensitive to resonance with external loading frequencies [1,2]; the detection of structural damage [3-5]; the tuning/designing of resonant vibration absorbers [6], meta-structures [7], and dynamic energy harvesters [8] for suppressing structural vibrations; the performance assessment of structures equipped with dynamic vibration absorbers [9]. In this regard, there is scope in developing cost-efficient modalities for on-site estimation of natural frequencies in existing/as-built engineering structures. This aim is widely pursued in practice via linear system identification techniques relying on measuring solely response acceleration time-histories collected from vibrating structures under operational/ambient unmonitored low-amplitude broadband excitations within the so-called operational modal analysis (OMA) framework [10]. Moreover, over the past two decades, wireless sensors/accelerometers have been heavily explored to further support the considered aim within the OMA framework as they enable rapidly deployable and low up-front cost field instrumentation compared to arrays of wired sensors [11-12].

Still, wireless sensors are constrained by frequent battery replacement requirements leading to increase maintenance costs while their bandwidth transmission limitations pose restrictions to the amount of acceleration measurements that can be reliably transmitted. To this end, it has been recently established that the above disadvantages of wireless sensors may be alleviated by developing compressive system identification approaches using acceleration measurements sampled at rates significantly below the nominal application-dependent Nyquist rate [13-22]. However, no particular provision is taken by any of the developed approaches for accurately resolving structural natural frequencies from the low-rate (sub-Nyquist) sampled acceleration measurements. Specifically, some of the approaches focus on estimating vibrational mode shapes

directly from sub-Nyquist measurements with natural frequencies seen as by-products or completely overlooked [14,15]. In other approaches, the sub-Nyquist sampled data are post-processed using various off-line computational techniques to recover/estimate either Nyquist-sampled time-histories [13,16,19] or their Fourier-based power spectral density function (PSD) [17,18,20-22] from which natural frequencies may be estimated using standard time-domain or frequency-domain OMA system identification, respectively. Clearly, in this setting, the accuracy by which natural frequencies are extracted depends on the quality/faithfulness by which time-domain or frequency-domain response acceleration information is recovered from the sub-Nyquist measurements. In this regard, note that, with the exception of the approach in [21], all sub-Nyquist system identification techniques rely on the compressive sensing (CS) paradigm [23] involving randomly sampled in time measurements whose (sub-Nyquist) sampling rate for faithful time/frequency domain information recovery or modal properties extraction depends on the acceleration signals sparsity. The latter is loosely defined as the number of significant/non-zero signal coefficients on a given basis. Therefore, the sparser the signal is, the lower the sampling rate (or equivalently the higher compression rate) can be practically considered using CS-based approaches. In this respect, these approaches are sensitive to naturally occurring broadband noise in response acceleration signals, which typically reduce signal sparsity [16], and ideally require additional knowledge of the signal structure [19] and/or statistical data post-processing [16,17], assuming the availability of large number of measurements, for efficient denoising and for setting appropriate sampling rates [20].

To overcome the above signal sparsity considerations for system identification with sub-Nyquist acceleration measurements, the authors proposed a power spectrum blind sampling approach [21] which relies on sub-Nyquist non-uniform in time deterministic multi-coset data acquisition to estimate the (PSD) matrix of stationary response acceleration signals treated as realizations of a multi-dimensional stationary stochastic process without imposing any sparsity

conditions. Whilst the latter approach does not return acceleration time-series, it achieves quality mode shape estimation via standard frequency domain OMA techniques at lower (sub-Nyquist) sampling rates compared to standard CS techniques even for noisy signals [20]. Along these lines, herein, a sparse-free structural system identification approach is put forth to estimate natural frequencies of existing linearly vibrating structures exposed to unmeasured broadband/white noise, within the OMA framework, from response acceleration measurements sampled at rates significantly below the nominal Nyquist rate. The approach couples the deterministic sub-Nyquist co-prime sampling scheme introduced in [24] with the standard multiple signal classification (MUSIC) algorithm (*e.g.*, [25]) to estimate the frequencies of structural response acceleration signals assuming a random multi-tone signal model. In this manner, the spectral estimation problem is cast in the time-domain rather than in the spatial domain pertaining to the direction of arrival problem in telecommunication applications [26] (i.e., detection of the direction of impinging signals by judicially deploying antenna arrays in space).

At the back-end (post-processing), the proposed approach benefits from the inherent super-resolution and denoising capabilities of the MUSIC algorithm yielding a pseudo-spectrum which is *known* to outperform conventional Fourier-based spectral estimators for extracting natural frequencies in vibration-based system identification applications using ordinary Nyquist-sampled data [27,28]. At the front-end (acquisition), the approach uses co-prime deterministic non-uniform in time low-rate sampling which does not rely on any signal sparsity conditions treating the acquired signals as wide-sense stationary stochastic processes. The adopted sampling scheme utilizes two conventional uniform in time sampling units (analog-to-discrete converters) per sensor operating at different *a priori* selected sub-Nyquist rates such that significantly fewer measurements are acquired cumulatively in time by both units than from a single sensor operating at Nyquist rate. In the numerical part of this work, different co-prime sampling schemes achieving different data compression (sub-Nyquist sampling rates) are considered to sample computer-generated response

acceleration signals from white noise excited structures with closely-spaced modes as well as weakly-excited modes. The signals are contaminated by different levels of additive white noise and attention is focused on assessing the potential of the proposed approach supported by the super-resolution and denoising attributes of MUSIC estimator to resolve the natural frequencies for various sub-Nyquist sampling rates and signal-to-noise ratios. Moreover, motivated by recent OMA-based approaches for rapid condition assessment of instrumented structures in the aftermath of earthquake events [29-32], a further numerical study is undertaken aiming to infer relatively light structural damage in frame-like buildings due to earthquake excitations based on shifts to the resonant frequencies estimated through the proposed sub-Nyquist MUSIC spectral approach applied before and after the seismic event.

In the remainder of this paper, Section 2 outlines the adopted co-prime sampling for autocorrelation estimation of stationary stochastic processes and reviews the mathematical details of the MUSIC algorithm. Section 3 considers a simulation-based approach to generate sub-Nyquist co-prime sampled noisy response acceleration measurements of white-noise excited structures with arbitrary number of natural frequencies and appraises the potential of the proposed approach to resolve closely-spaced and weakly excited vibration modes. Section 4 appraises the applicability of the approach for detecting light earthquake-induced structural damage from slight shifts in natural frequencies between the healthy (pre-earthquake) and damaged (post-earthquake) states. Finally, Section 5 summarizes concluding remarks.

2 Mathematical Background of Proposed Method

2.1 *Co-prime sampling and auto-correlation estimation of stationary stochastic processes*

Let $x(t)$ be a real-valued wide-sense stationary band-limited stochastic process assuming a spectral representation by a superposition of R sinusoidal functions with frequencies f_r, real amplitudes B_r, and uncorrelated random phases θ_r uniformly distributed in the interval $[0, 2\pi]$. That is, [33]

$$x(t) = \sum_{r=1}^{R} B_r \cos(2\pi f_r t + \theta_r)\,. \tag{1}$$

For the purposes of this work, the above multi-tone random signal model is interpreted as an "archetype" response acceleration process attained at some particular location of a broadband/white-noise excited linear structural system within the OMA framework. The system has R degrees of freedom (DOFs), observable at the location of consideration, with f_r (r=1,2,…,R) structural natural frequencies. This signal model is motivated by the fact that response time-histories of linear vibrating structures under low-amplitude ambient excitation have well-localized energy in the frequency domain centered at the structural natural (resonant) frequencies (e.g., [34]) and, in this respect, the model proved to be adequate for CS-based modal analysis in a previous study [14].

Co-prime sampling assumes that the process $x(t)$ is simultaneously acquired by two sampling units, operating at different (sub-Nyquist) sampling rates, $1/(N_1T_s)$ and $1/(N_2T_s)$, where N_1, N_2 are co-prime numbers ($N_1 < N_2$), and $1/T_s = 2f_{max}$ is the Nyquist sampling rate with $f_{\max}$ being the highest frequency component in Eq. (1) [24]. The process $x(t)$ is then divided in time blocks of $(2N_1\text{-}1)N_2T_s$ duration and, within each such block, only $2N_1+N_2\text{-}1$ samples are retained from a total number of approximately $2(N_1+N_2)\text{-}1\text{-}N_2/N_1$ available measurements. The retained samples of $x(t)$ from the two different sampling units are

$$\begin{aligned} x_1[k] &= x\left(kN_1T_s\right) = \sum_{r=1}^{R} B_r \cos(2\pi f_r kN_1T_s + \theta_r) + n_1[k], \quad k \in \{0,\ldots,N_2-1\} \\ x_2[\ell] &= x\left(\ell N_2T_s\right) = \sum_{r=1}^{R} B_r \cos(2\pi f_r \ell N_2T_s + \theta_r) + n_2[\ell], \quad \ell \in \{1,\ldots,2N_1-1\} \end{aligned} \tag{2}$$

where $n_1[k]$ and $n_2[\ell]$ are zero-mean uncorrelated Gaussian white noise sequences with common variance σ_n^2 associated with errors/noise introduced during sampling to the otherwise theoretically "noiseless" stochastic process in Eq.(1). In this setting, N_2 samples are obtained from the first sampler operating at sampling rate $1/(N_1T_s)$ and $(2N_1\text{-}1)$ samples are obtained from the second sampler operating at sampling rate $1/(N_2T_s)$. Overall, an average sub-Nyquist sampling rate of

$$f_{avg} = \frac{1}{N_1 T_s} + \frac{1}{N_2 T_s} \tag{3}$$

is attained.

Notably, co-prime sampling strategy is not heuristic; it is shown in [24] that the difference set of numbers $\Omega = \{N_2\ell - N_1 k\}$ contains all possible integers within the range [-N_1N_2, N_1N_2], with some redundancy/repetition. Thus, the cross-correlation function of the sequences $x_1[k]$, $x_2[\ell]$, whose support involves all the time-lags included in the set Ω, can be estimated in the above range of interest once redundant terms (i.e., products of samples) are discarded.

To this aim, the sequences in Eq. (2) are first stacked in a vector $\mathbf{y}_q \in \mathbb{R}^{(2N_1+N_2-1)}$ constructed as

$$\mathbf{y}_q = \left[x_1^{\mathrm{T}}\left[2N_2 q + k\right] \quad x_2^{\mathrm{T}}\left[2N_1 q + \ell\right] \right]^{\mathrm{T}} = \sum_{r=1}^{R} B_r \ \mathbf{e}(f_r) \ \cos(2\pi f_r N_1 N_2 q T_s + \theta_r) + \mathbf{n}, \quad q \in \{1, 2, ...\} \tag{4}$$

where the superscript "T" denotes vector/matrix transposition, $\mathbf{n} \in \mathbb{R}^{(2N_1+N_2-1)}$ is the vector collecting the sampling noise terms, and $\mathbf{e}(f_r) \in \mathbb{R}^{(2N_1+N_2-1)}$ is given as

$$\begin{aligned} \mathbf{e}(f_r) = \big[& 1 \quad \cos(2\pi f_r \ N_1 T_s) \quad \cdots \quad \cos(2\pi f_r (N_2 - 1) T_s) \\ & \cos(2\pi f_r \ N_2 T_s) \quad \cdots \quad \cos(2\pi f_r (2N_1 - 1) N_2 T_s) \big]^{\mathrm{T}} \end{aligned} \tag{5}$$

Importantly, in Eq. (4), the inclusion of the non-negative integer index $q \in \mathbb{Z}^*$ allows for arbitrarily placing the co-prime sampling block in time (*e.g.*, for q=0 the time block starts at t=0 and corresponds to the block considered in Eq. (2)). Therefore, an arbitrary large number of blocks (and corresponding vectors $\mathbf{y}_q$) can be used for sampling the theoretically infinitely long stationary process $x(t)$. The position of each block in time depends on the adopted values of q. The autocorrelation matrix of $\mathbf{y}_q$ is given as

$$\mathbf{R}_{\mathbf{yy}} = \mathrm{E}\left\{\mathbf{y}_q \ \mathbf{y}_q^{\mathrm{T}}\right\} = \sum_{r=1}^{R} B_r^2 \ \mathbf{e}(f_r) \ \mathbf{e}^{\mathrm{T}}(f_r) + \sigma_n^2 \mathbf{I} \tag{6}$$

in which $\mathbf{I} \in \mathbb{R}^{(2N_1+N_2-1)\times(2N_1+N_2-1)}$ is the identity matrix, while the mathematical expectation operator E{·} averages over *q*. That is, the matrix $\mathbf{R}_{\mathbf{yy}}$ in Eq. (6) is computed by averaging over all the time blocks considered within a Monte Carlo-based context.

Next, repeated (redundant) terms in the vector defined in Eq.(5), whose number increases with increasing N_1 and/or N_2, are systematically eliminated by extending the approach discussed in [26] for the case of spatial processes (direction of arrival problem), to treat the herein addressed problem of temporal frequency estimation. This is achieved by stacking the autocorrelation matrix in Eq. (6) in a column vector, $\mathbf{r}_\mathbf{y} = \text{vec}\left(\mathbf{R}_{\mathbf{yy}}\right)$, with $\mathbf{r}_\mathbf{y} \in \mathbb{R}^{(2N_1+N_2-1)^2\times 1}$. Then, the elements of $\mathbf{r}_\mathbf{y}$ are truncated within the range $[-N_1N_2, N_1N_2]$ while repeated terms are eliminated. The remaining elements are re-organised so that the integer indices of the exponential terms in Eq. (5) are sorted in increasing order with no repetition. The thus constructed reduced autocorrelation vector $\hat{\mathbf{r}}_\mathbf{y}$ is subsequently divided into $i=\{1,2,\ldots, N_1N_2+1\}$ overlapping subarrays, $\hat{\mathbf{r}}_{\mathbf{y}_i}$, each consisting of (N_1N_2+1) elements, which are averaged as in

$$\mathbf{R}_{ss} = \frac{1}{N_1N_2+1}\sum_{i=1}^{N_1N_2+1} \hat{\mathbf{r}}_{\mathbf{y}_i}\hat{\mathbf{r}}_{\mathbf{y}_i}^T . \tag{7}$$

From the numerical analysis viewpoint, the above described elimination of redundant terms increases the rank of the matrix in Eq.(6) yielding the full-rank autocorrelation matrix $\mathbf{R}_{ss} \in \mathbb{R}^{(N_1N_2+1)\times(N_1N_2+1)}$ in Eq.(7). In the following section, the latter matrix is used as input to the MUSIC super-resolution spectral estimator to detect the *R* frequencies f_r, (r= 1,2,…,R), of the considered stochastic process $x(t)$.

2.2 *Multiple signal classification (MUSIC) algorithm for natural frequencies estimation*

The MUSIC method for spectral content estimation yields a super-resolution "spiky" pseudo-spectrum by relying on the eigenvalue decomposition of autocorrelation matrices estimated by field

measurements [25]. Herein, MUSIC is applied to the autocorrelation matrix $\mathbf{R}_{ss}$ in Eq. (7), which is decomposed as in

$$\mathbf{R}_{ss} = \sum_{i=1}^{R} (\lambda_i + \sigma_\varepsilon^2)\mathbf{v}_i \mathbf{v}_i^{\mathrm{T}} + \sum_{i=R+1}^{N_1 N_2 + 1} \sigma_\varepsilon^2 \mathbf{v}_i \mathbf{v}_i^{\mathrm{T}} \tag{8}$$

where the eigenvectors $\mathbf{v}_i$ are orthonormal, *i.e.* $\mathbf{v}_i \mathbf{v}_j^{\mathrm{T}} = 0$ for $i \neq j$. The first term in Eq. (8) represents the signal sub-space with R eigenvalues $(\lambda_i + \sigma_\varepsilon^2)$, i=1,…,R, and R principal eigenvectors spanning the same subspace with the signal vector in Eq. (5). The second term corresponds to the noise sub-space with (N_1N_2-R) identical eigenvalues σ_ε^2, and (N_1N_2-R) eigenvectors. Then, the unbiased MUSIC pseudo-spectrum estimator is defined as

$$G_{MUSIC}(f) = \frac{1}{\mathbf{e}^{\mathrm{T}}(f) \cdot \left(\sum_{i=R+1}^{N_1 N_2 + 1} \mathbf{v}_i \mathbf{v}_i^{\mathrm{T}} \right) \cdot \mathbf{e}(f)}. \tag{9}$$

The above estimator becomes theoretically infinite at f=f_r, that is, at the location of the structural natural frequencies (i.e., the frequencies in the stochastic process of Eq.(1)) due to the following orthogonality condition between the signal vectors and the noise sub-space

$$\mathbf{e}^{\mathrm{T}}(f_r) \cdot \left(\sum_{i=R+1}^{N_1 N_2 + 1} \mathbf{v}_i \right) = 0, \quad \text{for } r = \{1, ..., R\}. \tag{10}$$

Practical numerical implementation, though, involves errors in approximating the solution of the eigenvalue problem in Eq. (8) and, therefore, Eq. (9) takes on finite values observing sharp peaks at each f_r and resulting in a spectrum-like shape (pseudo-spectrum). Note that MUSIC approaches requires an *a priori* assumption on the number of R signal components, while it involves increased computational demand in solving the eigenvalue decomposition in Eq. (8) for increased R. Nonetheless, the benefit of utilizing MUSIC to the full-rank matrix in Eq.(7) lies on its capability to capture up to $R \leq N_1N_2$ natural frequencies in noisy response acceleration signals acquired using the

co-prime sampling strategy at the low f_{avg} rate in Eq. (3) with nominal frequency resolution (i.e., frequency domain discretization step) of

$$f_{res} = \frac{1}{N_1 N_2 T_s} . \tag{11}$$

In the next two sections numerical examples are provided to appraise the potential of the proposed approach to discriminate closely-spaced structural natural frequencies as well as to detect small changes to natural frequencies interpreted as damage indices for various N_1 and N_2 pairs of values.

3 Identification of closely-spaced natural frequencies from noisy acceleration data

In this section, the proposed co-prime sampling with MUSIC spectral estimator approach is numerically assessed to estimate closely-spaced resonant frequencies of white-noise excited structures modelled as multi-degree-of-freedom (MDOF) dynamic systems. This is facilitated by considering a simulation-based framework to generate the pertinent noisy response acceleration time-histories. In particular, the framework allows to model physically implementable MDOF structural systems with arbitrarily pre-specified modal properties: modal damping, natural frequencies and spectral amplitudes at resonant frequencies. In this manner, realistic structural systems with closely spaced modes are defined without having to refer to a physical model (actual structure or lab specimen) or to a finite element model. The presentation begins with describing the simulation framework and proceeds with furnishing and discussing numerical results from application of the proposed method for various co-prime sampling number settings N_1 and N_2.

3.1 *Simulation framework for noisy co-prime-sampled response acceleration signals generation*

Consider a viscously-damped linear MDOF structural system with R modes of vibration, excited by zero-mean Gaussian white-noise band-limited to f_{max} with unit amplitude power spectral density

(PSD). Let $x(t)$ be the real-valued response/output acceleration process along a single monitored DOF of the MDOF system. The input-output PSD relationship is expressed as

$$G_x(f) = G_w(f)\left|H(f)\right|^2 \simeq \left|H(f)\right|^2, \tag{12}$$

where $H(f)$ is the frequency response function (FRF) of the MDOF system termed as accelerance in the field of modal testing [35]. The output PSD can be written as [36]

$$G_x(f) = f^4 \sum_{r,s=1}^{R}\left[A_{rs} \frac{(f_r^2 - f^2)(f_s^2 - f^2) + 4f^2 f_r f_s \zeta_r \zeta_s}{[(f_r^2 - f^2)^2 + (2ff_r\zeta_r)^2]\cdot[(f_s^2 - f^2)^2 + (2ff_s\zeta_s)^2]}\right], \tag{13}$$

in which f_r and f_s are the natural frequencies, and ζ_r and ζ_s are the damping ratios of the r-th and s-th modes of vibration of the MDOF system, respectively, while the modal amplitude A_{rs} is a parameter dependent on the modal participation factors and on the monitored DOF.

To appraise the potential of the proposed approach to estimate the R natural frequencies of the considered white-noise excited MDOF structural system with known modal properties (f_r, A_r, ζ_r) from the monitored $x(t)$ response acceleration, the simulation-based assessment framework shown in Fig. 1 is devised. The framework takes as input the continuous-time (analog) PSD in Eq. (13). This represents the "target" PSD which is, then, replaced by a surrogate discrete-time auto-regressive moving average (ARMA) filter of order (P, Q) given by the transfer function

$$\hat{H}(e^{i2\pi fT_s}) = \frac{\sum_{\ell=0}^{Q} c_\ell e^{-\ell i 2\pi f T_s}}{1 + \sum_{k=1}^{P} b_k e^{-ki2\pi fT_s}}, \tag{14}$$

where b_k , k=(1,2,…,p), and c_ℓ , $\ell = (0,1,...,q)$ are the ARMA filter coefficients. These coefficients are derived by using the auto/cross-spectrum correlation matching method [37], widely used for spectrum compatible simulation applications (*e.g.*, [38,39]) such that the error function

$$\varepsilon = \int_{-f_{\max}}^{f_{\max}} \left| G_x(\omega) - \left|\hat{H}(e^{i2\pi fT_s})\right|^2 \right|^2 df \tag{15}$$

is minimized.

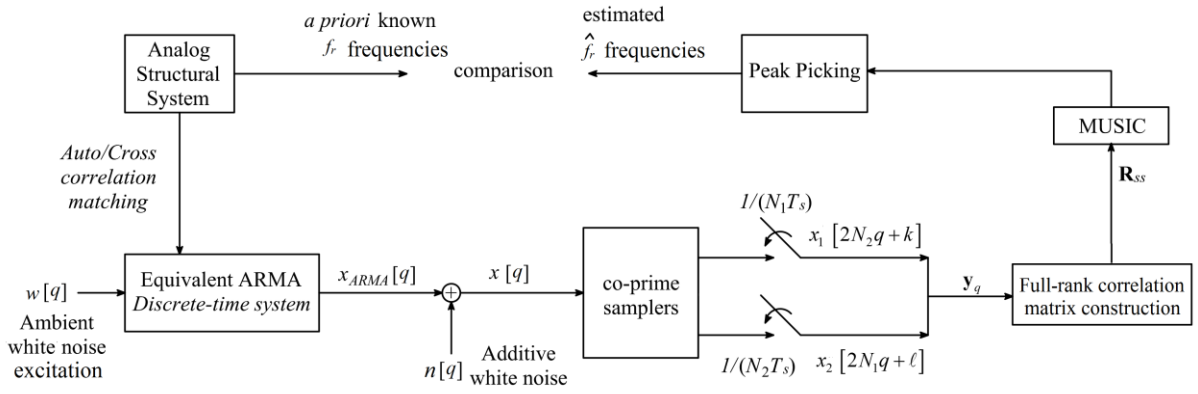

Figure 1. Simulation-based assessment framework for the proposed natural frequencies identification approach in OMA applications

Next, the thus defined ARMA filter is excited by white-noise sequences, $w[q]$, to generate a discrete-time Nyquist-sampled realization, $x_{ARMA}[q]$, of an underlying stochastic process representing the acceleration response of the original MDOF structural system with properties (f_r, A_r, ζ_r). This is achieved by recursively computing each q sample in $x_{ARMA}[q]$ based on past observation and adding a convolution term related to the white noise input $w[q]$, *i.e.*,

$$x_{ARMA}[q] = -\sum_{k=1}^{P} b_k x_{ARMA}[q-k] + \sum_{\ell=0}^{Q} c_\ell w[q-\ell]\,. \tag{16}$$

The above sequence is further contaminated by additive white noise to model ambient/environmental noise observed in field recorded response acceleration signals as shown in Fig.1. Notice that the noise is added to the signal prior to sampling, making it non-compressible within the CS-based context (e.g., [Huang et al]), and not to the back-end of the samplers as considered in section 2.1. In this respect, sufficiently long discrete-time sequences are considered in simulation to ensure that this difference between theory and numerical implementation emulating real-life conditions does not influence results. The derived noisy acceleration response signals, $x[q]$, are then and co-prime sampled as detailed in section 2.1 and the full-rank autocorrelation matrix in Eq. (7) is constructed. The latter is further treated by the MUSIC pseudo-spectral estimation algorithm in section 2.2, yielding a de-noised spectrum attaining large values near the location of resonant frequencies.

Therefore, estimates $\hat{f}_r$ of the natural frequencies f_r are extracted by application of peak picking [10] to the MUSIC spectrum and the quality/accuracy of the proposed approach for natural frequencies identification is assessed by gauging percentage difference among the obtained $\hat{f}_r$ and the known f_r, r=1,2,…,R.

3.2 *Adopted structural systems and noisy response acceleration signals generation*

Two different MDOF structural systems with R=3 DOFs are examined having two equally-excited closely-spaced modes of vibration and a third weakly excited mode attaining a low FRF amplitude. These systems represent cases of structures for which resolving natural frequencies with high accuracy from response acceleration signals is a rather challenging task, especially in noisy environments [35]. Specifically, both the considered systems have the same critical modal damping ratio of ζ_r =5% (r=1,2,3) for all modes and the same modal amplitudes A_{rs}=1 (r,s= 1,2,3) in Eq.(13) except for A_{12}=A_{21}=2 and A_{33}=0.25. Further, both systems have common second and third natural frequencies f_2=70Hz, and f_3= 120Hz, but different first natural frequency, f_1= 66Hz for structure 1 and f_1= 67Hz for structure 2, such that the first two modes of structure 2 are more closely-spaced compared to structure 1 (i.e., (f_2-f_1)/f_1 is about 6% for structure 1 and only 4.5% for structure 2). Figure 2 plots the PSDs in Eq. (13) for the two structures. Note in passing that, purposely, both the above systems considered to demonstrate the accuracy of the proposed natural frequencies identification approach correspond to very high-frequency (stiff) structures (or vibration modes). This is because monitoring/identification of such structures require high Nyquist sampling rates ($1/T_s$) resulting in arduous energy consumption and transmission payloads in case of using wireless sensors/accelerometers. For such monitoring applications, reducing the number of acquired acceleration measurements (or equivalently response acceleration sampling rate) for effective system identification, which is the main thrust of the herein proposed approach, is practically quite

meritorious as it will significantly prolong sensor battery lifetime thus reducing the frequency of battery replacement and the associated maintenance costs [14, 19-22].

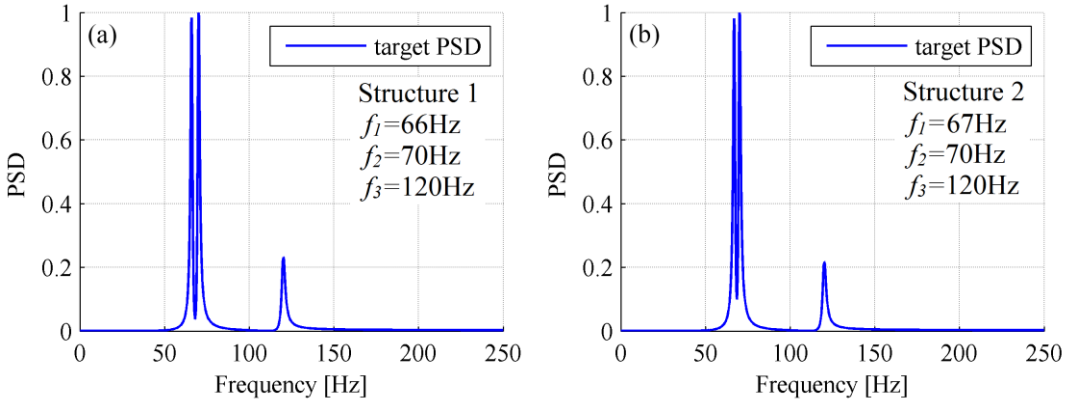

Figure 2. Normalized target PSDs in Eq.(13) for the two adopted 3-DOF structural systems.

Following the simulation-based framework in Fig.1, the PSDs of Fig.2 are first replaced by surrogate discrete-time ARMA filters of order (120, 12) which is then subjected to a clipped white-noise excitation of 20s duration, sampled at a Nyquist rate of F_s=1/T_s=500Hz (*i.e.*, T_s=0.002s). The generated discrete-time ARMA response signals are corrupted by additive white noise at five different signal-to-noise ratios (*SNR*s) ranging within [0, 20] dB to assess the influence of the accuracy of the proposed approach as signal noise level increases. In this work, the *SNR* is defined as

$$SNR = 10 \cdot \log_{10}\left(\frac{\sigma_x^2}{\sigma_n^2}\right), \tag{17}$$

where σ_x^2 and σ_n^2 are the signal and noise variance, respectively. Therefore, the case of *SNR*=0 dB corresponds to $\sigma_n^2 = \sigma_x^2$, that is, the signal and the noise are of equal power, representing extreme noise conditions, while the case of *SNR*=20 dB represents low noise level with $\sigma_n^2 = 0.01\sigma_x^2$.

3.3 *Co-prime data sampling at different sub-Nyquist rates and correlation matrix estimation*

The previously described noisy discrete-time acceleration response signals are co-prime sampled as detailed in section 2 using four different sampling settings (i.e., different N_1 and N_2 pairs of prime

numbers) listed in Table 1. The same table reports the f_{avg} sub-Nyquist sampling rate in Eq. (3) as percentage of the Nyquist rate, the nominal spectral resolution f_{res} in Eq.(11) and the size of the correlation matrix $\mathbf{R}_{ss}$ in Eq.(7). It further reports the number of blocks, K, and the length of each such block used in computing the autocorrelation matrix $\mathbf{R}_{yy}$ in Eq.(6), as well as the total number of compressed (co-prime samples) considered in obtaining $\mathbf{R}_{yy}$. To illustrate the calculations involved, consider the co-prime sampling scheme with N_1=7 and N_2=11. The underlying assumption is that two samplers are deployed per recording location to acquire uniform samples of the same acceleration response signal (in time), with sampling rates equal to $1/(7T_s)$ and $1/(11T_s)$, respectively. The two samplers accumulate measurements at an average rate of $1/(7T_s) + 1/(11T_s)$ samples per second, which is about 76.6% lower than the Nyquist rate. Further, the assumed co-prime numbers define the cross-difference set $\Omega = \{11\ell - 7k,\ k \in [0,10], \ell \in [1,13]\}$, which includes all discrete time lags within the support [-77, 77] of the cross-correlation function between the measurements of the two sensors as detailed in section 2.1. It is further assumed that the measured acceleration signal is divided in K non-overlapping time-blocks that are used for the computation of the autocorrelation matrix in Eq. (6). Each block contains $(2N_1\text{-}1)\times N_2$=143 Nyquist samples from which only $2N_1+N_2\text{-}1$= 24 samples are taken to populate the $\mathbf{R}_{yy} \in \mathbb{R}^{24\times 24}$ matrix in Eq. (5). Next, the full-rank matrix $\mathbf{R}_{ss} \in \mathbb{R}^{78\times 78}$ in Eq. (7) is constructed from the coprime-sampled (compressed) measurements. Finally, the MUSIC pseudo-spectrum in Eq. (9) is evaluated. For the other sub-Nyquist sampling cases in Table 1 the pertinent co-prime sampling parameters and correlation estimators are defined in a similar manner as above.

Table 1. Co-prime sampling specifications

Co-prime numbers (N_1, N_2)	Sampling rate f_{avg} below Nyquist rate	Nominal spectral resolution f_{res} [Hz]	Size of matrix $\mathbf{R}_{ss}$	Nyquist samples per block	Number of blocks K considered	Total number of co-prime measurements
(3,7)	52.4%	23.81	22x22	35	285	3420

(5,7)	65.7%	14.29	36x36	63	158	2528
(7,11)	76.6%	6.49	78x78	143	69	1656
(7, 13)	78.0%	5.49	92x92	169	59	1534

From a practical viewpoint, it is important to note that the K block length depends on the co-prime numbers and, thus, is different for each sampling scheme considered. To this end, in establishing a meaningful comparison among sampling schemes, the assumed number of blocks K observed is set such that the total length of the observation window remains roughly the same for all four sampling schemes. Under this assumption, the last column of the table reports the total number of samples acquired by co-prime sampling: ultimately, this is the number of measurements that need to be transmitted by a (wireless) sensor in an actual monitoring deployment. It is seen that higher co-prime numbers improves both frequency resolution and data compression which, under the assumption of constant latency, results in fewer measurements. These benefits come at the expense of a larger eigenvalue problem to solve (size of matrix $\mathbf{R}_{ss}$) to obtain the MUSIC pseudo-spectrum which increases computational cost. Nevertheless, this operation can be undertaken off-line at a server station collecting/receiving compressed co-prime data from all sensors and, therefore, does not compromise the efficiency of the sensors deployment.

3.4 *Identification of closely-spaced structural resonances from noisy data*

Figure 3 and 4 plot the obtained MUSIC pseudo-spectra for the two examined 3DOF structural systems in Figure 2 for all four co-prime sampling specifications of Table 1 and for all five *SNR* values. All spectra are normalized to unit amplitude to facilitate comparison and plotted along a horizontal axis labelled after the pertinent *SNRs*.

Gkoktsi K and Giaralis A (2020) A compressive MUSIC spectral approach for identification of closely-spaced structural natural frequencies and post-earthquake damage detection. *Probabilistic Engineering Mechanics*, accepted: 27/12/2019.

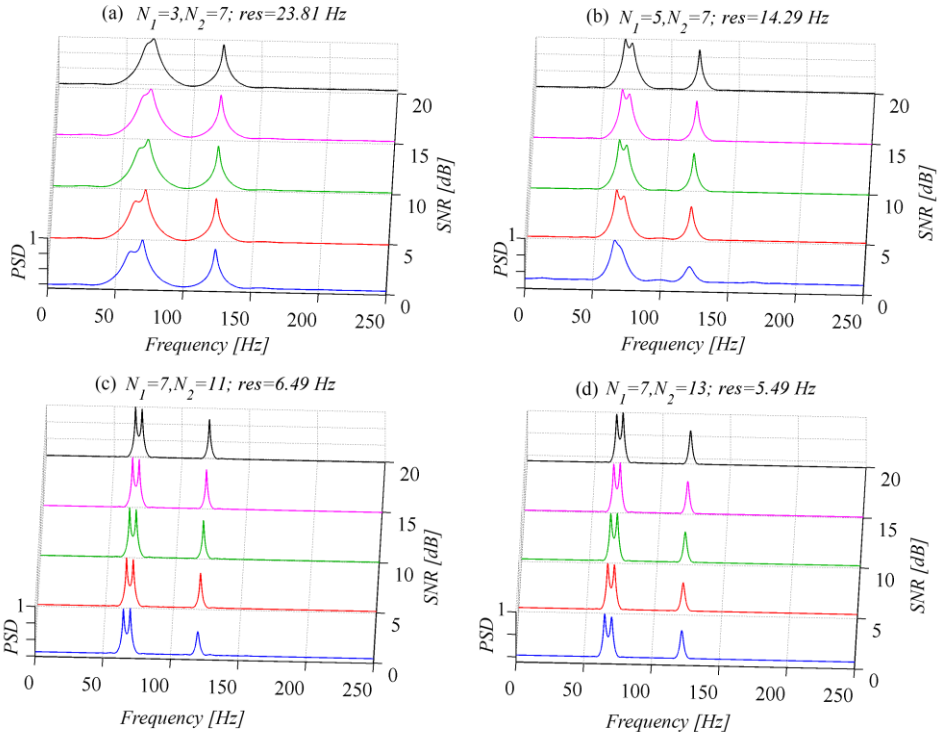

Figure 3. MUSIC pseudo-spectra of structure 1 in Fig.2(a) obtained for co-prime sampling specifications of Table 1 and for 5 different SNR values.

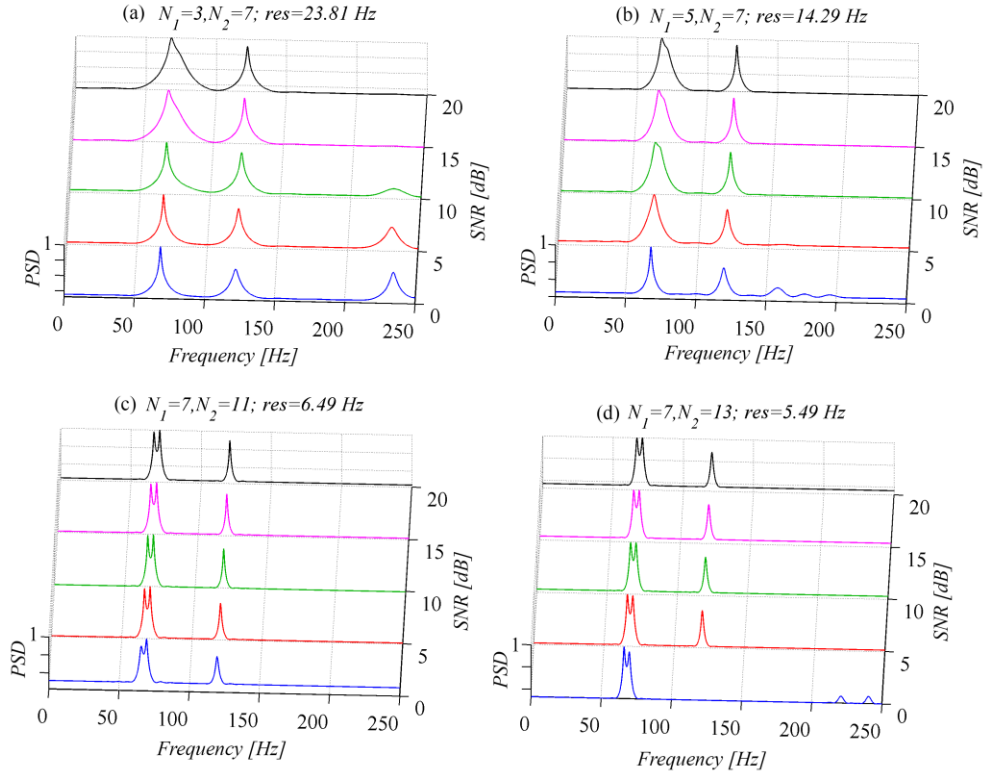

Figure 4: MUSIC pseudo-spectra of structure 2 in Fig.2(b) obtained for co-prime sampling specifications of Table 1 and for 5 different SNR values.

From qualitative observation of the spectra in Figures 3 and 4, it is readily seen that the efficacy of the MUSIC pseudo-spectrum in extracting the two closely-spaced natural frequencies depends strongly on the frequency resolution achieved by the adopted co-prime sampling scheme. Specifically, the sampling scheme corresponding to the lowest frequency resolution cannot discriminate the closely-spaced frequencies of structure 1 in Fig.3(a); the closely-spaced resonant frequencies are merged yielding a single spectral peak at a frequency value of 70Hz. Still, the third high-frequency and least excited mode is retrieved at 120Hz. By increasing resolution in the (N_1=5, N_2=7) scheme, the two peaks of the closely-spaced frequencies become discernible at least for SNR>5dB. As the co-prime numbers increase, achieving higher resolution, the proposed approach yields sharper spectral peaks, capable to clearly discriminate the two closely-spaced natural frequencies as well as resolve the weakly excited mode of vibration with high accuracy. More importantly, this particular example shows that the estimator is practically immune to additive noise suggesting that the choice of the pair of co-prime numbers will be based on the trade-off between computational cost required in obtaining the eigenvalue decomposition in Eq.(7) and the number of the acquired co-prime measurements as seen in Table 1.

For the case of structure 2 (Figure 4) in which the first two modes lie closer than in structure 1 it is seen that higher resolution than the one achieved by the (N_1=5, N_2=7) co-prime sampling scheme is required to discriminate the closely-spaced frequencies: in Figs. 4(a) and 4(b) the closely-spaced resonant frequencies are merged yielding a single spectral peak at an averaged frequency value of 68.5Hz. Furthermore, it is seen that the combination of low resolution and high additive noise level, that is, for SNR<15dB and SNR<5dB for the co-prime sampling with pairs (3,5) and (3,7) respectively, leads to false frequency detection as spurious spectral peaks are observed at frequencies higher than 120Hz. Evidently, the MUSIC algorithm cannot effectively filter out large levels of additive noise as the order of the spectral decomposition in Eq.(8) reduces. Nevertheless, as the co-prime numbers increase to (N_1=7, N_2=11) and (N_1=7, N_2=13) pairs, achieving higher resolution, the

proposed approach yields sharper spectral peaks, capable to discriminate the two closely-spaced natural frequencies as well as resolve the weakly excited mode of vibration with high accuracy. As in the case of structure 1, the MUSIC estimator becomes practically immune to noise, yielding exactly the same performance for *SNRs* as low as 5dB. Note, however, that for the extreme noise case and for the (N_1=7, N_2=13) co-prime pair, the MUSIC algorithm becomes over-sensitive in terms of denoising and classifies the weakly excited mode as "noise" for the example structure 2. Even though this is only observed for unrealistically high additive noise, it calls for caution in selecting the co-prime number pairs in practical settings.

4 Application for natural frequency-based post-earthquake damage detection

In this section, an additional numerical study is undertaken to demonstrate the applicability and usefulness of the proposed system identification method in detecting relatively light structural damage induced to buildings by earthquakes. Herein, much more flexible structural systems than those examined in the previous section (Fig.2) are considered being representative of large-scale (civil) engineering structures for which wireless-sensor assisted OMA is practically mostly relevant [11]. Moreover, this numerical study is inspired by recent research work recognizing that structural damage detection techniques can facilitate timely condition assessment of multi-storey building structures instrumented for OMA in the aftermath of earthquake events (see e.g., [30-32]) to improve the resiliency of communities against the seismic hazard [40]. To this aim, the proposed approach is applied to estimate natural frequencies before (healthy state) and after (potentially damaged state) a seismic event within the standard OMA context (i.e., stationary excitation and linear structural response assumptions apply). Damage is inferred by (small) shifts in natural frequencies of the healthy and damaged structure assuming that environmental conditions, known to affect natural frequencies such as temperature and humidity, remain the same before and after the seismic event: a reasonable assumption to make given the short duration of

earthquakes (see also [32]). Notably, in this setting, the consideration of wireless sensors in conjunction with the proposed co-prime sampling plus MUSIC approach leading to reduced sensor energy consumption is practically quite beneficial as long-term/permanent structural monitoring deployments are required for the purpose. In such deployments reducing battery replacement frequency, and thus maintenance costs, becomes critical and may be a main criterion for installing a monitoring system in the first place (e.g., [13]).

4.1 Adopted structure and seismic action

In this numerical study, the planar 3-storey single-bay reinforced concrete (r/c) frame in Figure 5 is considered as a case-study structure with beams and columns longitudinal and transverse reinforcement as indicated in the figure. The nominal concrete strength is taken equal to 20MPa, while the characteristic steel yielding strength is f_{yk}=400MPa for both the longitudinal and transverse reinforcement and the steel hardening ratio is taken as f_{uk}/f_{yk}=1.15. In computing the axial forces carried by the columns, a gravitational uniform distributed load along the beams equal to 35 kN/m is assumed.

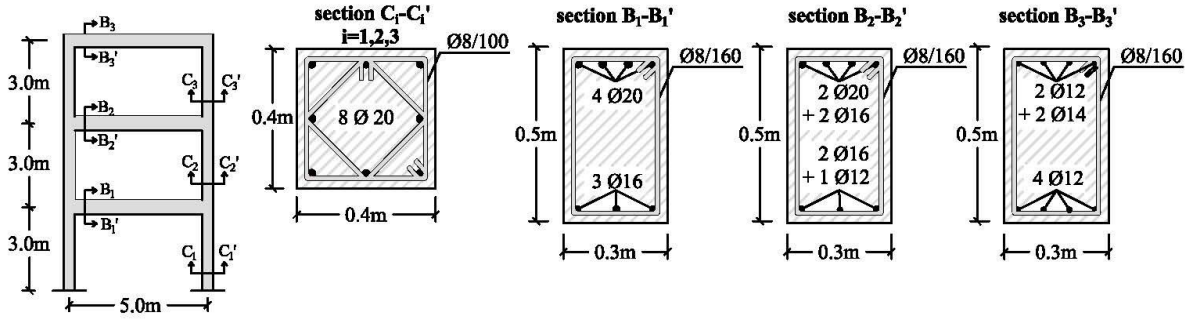

Figure 5. Adopted reinforced concrete case-study frame.

The structure in Fig.5 is exposed to the horizontal ground motion shown in Fig.6 unscaled as well as down-scaled by a factor of 0.5 to create two structural damage states of different severity. The unscaled record has peak ground acceleration (PGA) equal to 3.17m/s^2 and is characterized by high energy in a wide frequency range. The two different damaged states of the structure in Figure

5 are predicted through response history analysis (RHA) applied to a nonlinear finite element (FE) model of the case-study structure as detailed in the following sub-section.

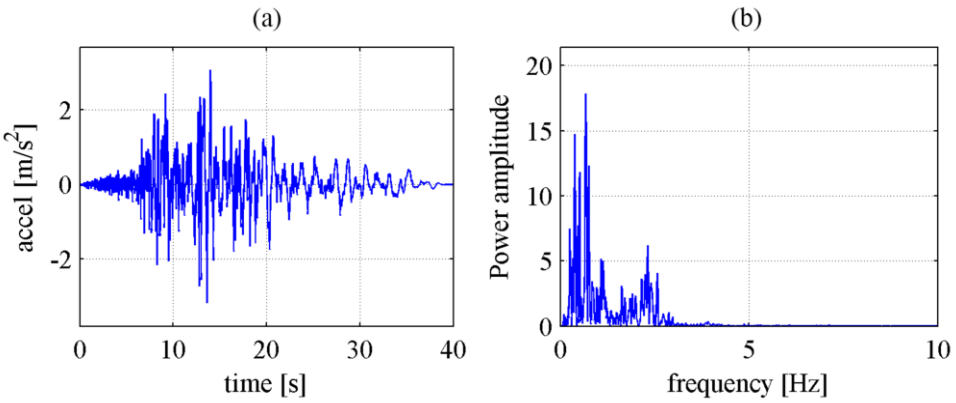

Figure 6. Horizontal ground motion component recorded at "Sanjo Shinbori" station during the Mw=6.8 Chuetsu-oki event (16.7.2007) in Japan: (a) Time-history, (b) Squared amplitude of Fourier spectrum [23]

4.2 Finite element modelling of earthquake-induced

Non-linear RHA is undertaken using the *Ruaumoko* FE software to quantify the structural damage induced to the structure in Figure 5 due to the earthquake excitation in Figure 6 scaled by a factor of 0.5 (damaged state 1) and its unscaled version (damaged state 2). To this aim, a non-linear lumped-plasticity FE model is developed, based on the material properties, geometry, and reinforcement detailing shown in Fig.5. This is accomplished by first conducting a section analysis to determine the values of the moment capacity- curvature pairs at yielding, M_y-φ_y, and at collapse, M_u-φ_u, at the critical (energy dissipation) zones of all the frame members (*i.e.*, ends of all beams and columns in Fig.5). Then, the secant flexural rigidity at yielding, $EI_y=M_y/\varphi_y$, corresponding to cracked reinforced concrete sections at all the critical zones is obtained. Table 2 reports the average EI_y values at the ends of all structural members.

Table 2. Average secant flexural rigidity at yielding, EI_y, at the ends of the frame structural members of Fig. 5

	Beams			Columns		
	1st storey	2nd storey	3rd storey	1st storey	2nd storey	3rd storey
EI_y [kNm^2]	23531	20719	16219	19709	18237	16573

The plastic hinge length of all critical zones is estimated by the empirical formula [41]

$$L_{pl} = \max \begin{cases} \min\left(0.2(\frac{f_{uk}}{f_{yk}} - 1)L_o, 0.08\right) + 0.022\, f_{yk} d_{bl} \\ 0.044\, f_{yk} d_{bl} \end{cases}, \quad (18)$$

where L_o is the shear span taken herein as half the structural member length, d_{bl} is the diameter of the longitudinal reinforcement, and f_{yk}, f_{uk}/f_{uk} are the steel strength and strain hardening ratio, respectively, given in the previous sub-section. In this study, Eq. (18) yields the value L_{pl}=0.352m for the critical zones in all beams and columns with the exception of the beam at the 3rd storey exhibiting plastic zones with L_{pl}=0.246m at both ends.

With moment capacity-curvature pairs at yielding, M_y-φ_y, and at collapse, M_u-φ_u, as well as plastic hinge lengths derived as detailed above, non-linear rotational springs with time-evolving moment-curvature, M-φ, relationship governed by the Takeda hysteretic model [42] are used to capture the behavior of the plastic hinges that may develop at the critical zones of the considered frame under seismic excitation. The sections of beams and columns in between the critical zones are modelled as linear-elastic with flexural rigidity equal to EI_y in Table 2.

Results from non-linear RHA to the above FE model show that for both the considered ground motion intensities all beam members yield while columns remain elastic. In this regard, the considered r/c frame exhibits the anticipated behavior of a code-compliant structure designed for earthquake resistance under nominal design earthquake scenario [43]. To further illustrate this point and to demonstrate the impact of scaling-down the considered ground motion by 0.5 in terms of non-linear response behavior, Fig.7 plots moment-curvature curves at the left plastic hinge on the beam of the 1st storey, for the two damaged states considered. Notably, the maximum curvature ductility in Fig.7(a) is close to unity (*i.e.*, μ_φ=1.45) associated with a very small structural damage near yield. From Fig.7, it is readily observed that maximum stiffness degradation occurs at the

maximum curvature ductility characterized by an effective flexural rigidity, EI_{eff} (slope of red dashed lines in Fig.7), smaller than the secant flexural rigidity at yielding, EI_y (slope of green dashed lines in Fig.7, also reported in Table 2). In this regard, the average ratio EI_{eff}/EI_y (flexural stiffness reduction factor) at the critical zones is herein considered to represent local earthquake-induced damage related to stiffness degradation as captured by the Takeda hysteretic model. Table 3 presents the thus defined stiffness reduction factors for the two considered damaged states, which yield smaller values within the second case pertaining to a seismic event of increased intensity. The increased severity of the second damage state reflects on lower values of stiffness reduction factors for the beams, while columns remain practically linear.

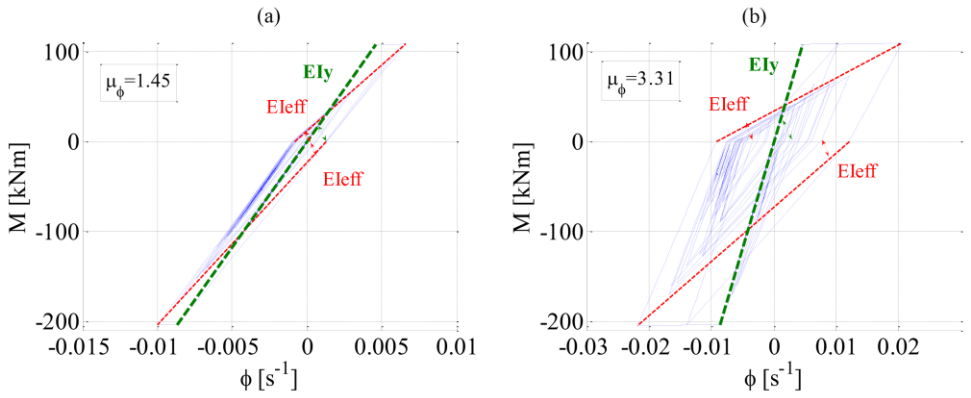

Figure 7. Moment-curvature (M-φ) hysteretic curves at the left plastic hinge of the 1st storey beam for (a) damage state 1 and (b) damage state 2.

Table 3. Flexural rigidity reduction factor (EI_{eff}/EI_y) at critical member zones of the structure in Figure 5 for the two different damage states considered due to different seismic intensity excitation

	Beams			**Columns**		
	1st storey	**2nd storey**	**3rd storey**	**1st storey**	**2nd storey**	**3rd storey**
Damaged state 1	0.71	0.53	0.46	1.00	1.00	1.00
Damaged state 2	0.21	0.15	0.17	1.00	1.00	1.00

Ultimately, the reduction factors of Table 3 are used to model earthquake-induced structural damage to the structure of Fig.5 due to the two different levels of seismic excitation considered. Specifically, two equivalent linear FE models are defined, corresponding to the two different damage states, in which the earthquake-induced damage is represented by means of the flexural stiffness reduction factors of Table 3. The latter are assigned to linear beam elements of length L_{pl} at the considered plastic hinge zones, while the remaining non-critical frame members exhibit the flexural rigidities in Table 3. Importantly, this modelling of local structural damage is deemed more realistic compared to the arbitrary reductions of floor stiffness (*i.e.*, along the whole length of structural members), commonly considered in the relevant literature **Error! Reference source not found.Error! Reference source not found.**. Further, the pre-eartquake/"healthy" state of the considered structure is modelled by a linear FE model with the secant flexural rigidities at yield presented in Table 2 assigned to the full length of structural members.

4.3 Post-earthquake damage detection

Linear RHA is undertaken for the three FE models defined in the previous sub-section (healthy plus two damaged states), using the same low amplitude white noise base excitation of 80s duration. A time discretization step of T_s=0.01s is taken corresponding to a Nyquist frequency of 50Hz. The considered excitation represents ambient wide-band noise input under operational conditions within the OMA context. A critical damping ratio of 5% for all modes of vibration is assumed in the analysis. Horizontal response acceleration signals at all floor levels are recorded at the Nyquist rate F_s=1/T_s= 100Hz (*i.e.*, 8000 Nyquist measurements per signal) and stored. They are treated as noise-free structural response acceleration time-histories due to ambient noise, field-recorded by sensors located at each floor. Further, these response signals are contaminated with additive Gaussian white noise at three different signal-to-noise ratios (*SNRs*): 10^{20}dB (practically noise-free case), 30dB, and 10dB.

The obtained discrete-time noisy response acceleration signals from the healthy and the two damaged states are co-prime sampled as detailed in section 2. Considering the optimal performance of the adopted pseudo-spectral estimator, it was deemed reasonable to select herein the co-prime numbers N_1=7 and N_2=11 along with the pertinent sampling values reported in Table 1. Thus, two co-prime samplers are assumed per recording location that operate on uniform sampling rates N_1=7 and N_2=11 times slower than Nyquist, respectively, yielding an average rate which is about 76.6% lower than Nyquist. In this numerical evaluation, the correlation matrix in Eq.(6) is computed from K=492 time-blocks. Each block contains 143 Nyquist samples from which only 24 samples are taken to populate the $\mathbf{R}_{yy} \in \mathbb{R}^{24\times24}$ matrix. It is noted that a certain level of overlapping between the considered time blocks occurs, given that the structural response acceleration signals are only 8000 Nyquist samples long. However, under the wide-sense stationary assumption and implied ergodicity in the data, this overlapping does not affect the obtained numerical results. Following the mathematical details in sub-section 2.1, the coprime-sampled (compressed) measurements are next used to derive the spatially smoothed correlation matrix $\mathbf{R}_{ss} \in \mathbb{R}^{78\times78}$ in Eq.(6). The latter is further treated by the MUSIC algorithm in sub-section 2.2 to compute the pseudo-spectral estimator in Eq. (8), assuming R=3 degrees of freedom in the measured response acceleration signals.

Compared to Fourier-based spectral estimators, MUSIC yields a pseudo-spectrum with sharp peaks corresponding to the natural frequencies of the white-noise excited 3-storey frame (following standard OMA and linear random vibrations considerations), while filtering out additive broadband noise. As an example aiming at system identification, Fig.8 plots the conventional periodograms (DFT-based spectral estimators) of Nyquist-sampled noisy response acceleration signals (at SNR=10dB), recorded at all floors of the healthy 3-storey white-noise excited structure. Figure 8 also superimposes the MUSIC pseudo-spectra, obtained from both Nyquist-sampled signals (broken line) and co-prime sampled signals (solid line). All spectra are

normalized to their peak amplitude to facilitate comparison. It is seen that it is not possible to extract the natural frequencies of the structure from the periodogram of the considered noisy signals sampled at the Nyquist rate (*e.g.* the 3rd natural frequency is masked by noise). However, the MUSIC pseudo-spectrum estimated from the co-prime sampled signals (using less than 76% measurements from the sub-Nyquist rate) can be readily used to detect the resonant frequencies of the structure with high resolution, even for this extreme noise level. More importantly, it is found that the MUSIC pseudo-spectrum derived from the Nyquist and the sub-Nyquist sampled signals practically coincide in this case. Thus, the signal information pertaining to the natural frequencies of the system is not lost due to a more than 76% signal compression at acquisition (sub-Nyquist sampling).

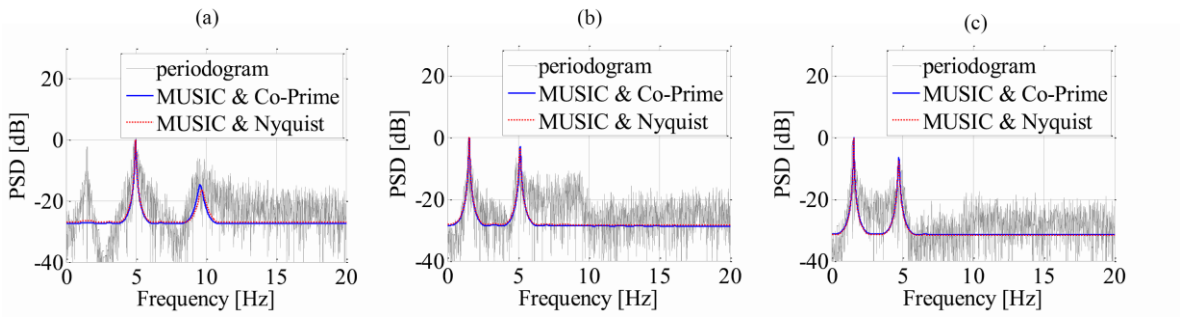

Figure 8. Spectrum estimation from noisy acceleration response signals with *SNR*=10dB at the (a) first, (b) second, and (c) third floor of the structure in Fig. 5 (healthy state) subject to 80s duration white noise base excitation

Having demonstrated numerically the capability of the MUSIC spectrum to identify structural resonant frequencies from the co-prime sampled signals buried in noise, structural damage detection is next pursued based on the shifts of the natural frequencies between the healthy state of the structure in Fig.5, and the two damaged states due to different levels of ground motion excitation, as detailed in previous sub-sections. For illustration, Figs. 9 and 10 plot the MUSIC spectra obtained by co-prime sampled measurements for damaged states 1 and 2, respectively, at all three floors (recording locations). The MUSIC spectra of co-prime sampled measurements from

the healthy state are superimposed in all panels of Figs. 9 and 10. In all plots, a shift of the natural frequencies towards smaller values is seen indicating structural damage. Expectedly, these shifts are smaller for damage state 1 (*i.e.*, lighter damage near yield pertaining to the scaled-down input ground motion), rendering the damage detection problem more challenging. It is further important to note that in each panel of Figs. 9 and 10 only two out of the expected three structural natural frequencies are detected. Specifically, the MUSIC spectra at the first floor do not capture the first (fundamental) natural frequency, while the spectra at the 2nd and the 3rd floor do not capture the highest (third) natural frequency. In this regard, the three natural frequencies, for each of the three different FE models considered, are estimated by averaging the natural frequency values obtained from the MUSIC spectra across all three floors. Tables 4 and 5 report the thus estimated three natural frequencies (*i.e.*, averaged over the three floors) for the different FE models and for three different *SNR* levels *i.e.* 10^{20}dB (practically noise-free case), 30dB, and 10dB. The "exact" natural frequencies obtained from standard modal analysis in *Ruaumoko* are also reported. It is seen that the MUSIC algorithm coupled with co-prime sampling can retrieve the underlying resonant frequencies of the adopted frame in the three considered structural states (*i.e.*, one healthy and two damage states, respectively), with a small error of 1-5% with respect to the exact solution. Tables 4 and 5 further report percentage differences computed between the natural frequencies of the healthy and the damaged states in all cases considered – a quantity that is used as an indicator of structural damage. Notably, the reported percentages derived from the co-prime MUSIC spectra yield almost the same values within the entire *SNR* range, and closely approximate the percentage differences retrieved from the exact modal values (*i.e.*, from the standard modal analysis in *Ruaumoko*). Thus, the numerical results show that the proposed methodology is capable to infer structural damage even in low-intensity earthquake excitations by capturing small changes to the natural frequencies while being practically insensitive to noise.

Gkoktsi K and Giaralis A (2020) A compressive MUSIC spectral approach for identification of closely-spaced structural natural frequencies and post-earthquake damage detection. *Probabilistic Engineering Mechanics*, accepted: 27/12/2019.

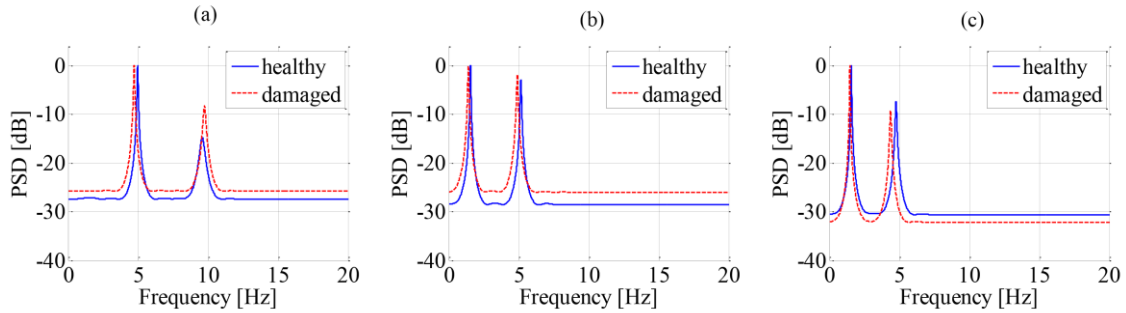

Figure 9. MUSIC pseudo-spectra with co-prime sampling of noisy acceleration response signals with SNR=10dB at the (a) first, (b) second, and (c) third floor for the healthy and the damaged state 1 structure

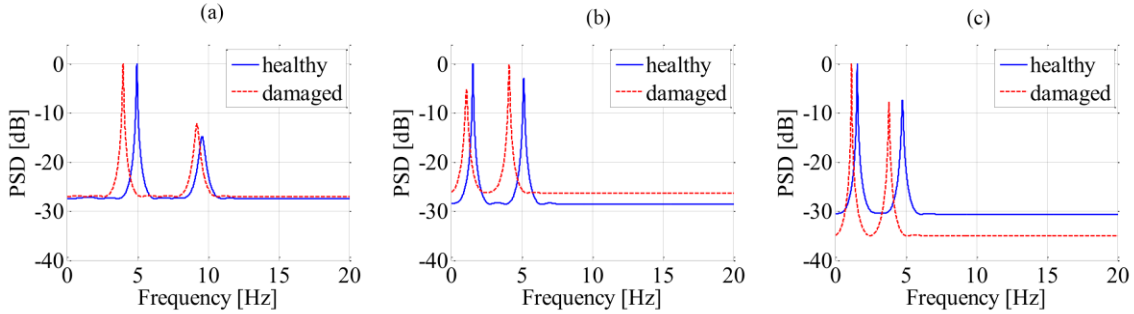

Figure 10. MUSIC pseudo-spectra with co-prime sampling of noisy acceleration response signals with SNR=10dB at the (a) first, (b) second, and (c) third floor for the healthy and the damaged state 2 structure

Table 4. Assessment of MUSIC spectra from co-prime sampled noisy measurements for damage detection based on structural natural frequency shifts: damage state 1

SNR [dB]	State*	f_1 [Hz]		df_1/f_1	f_2 [Hz]		df_2/f_2	f_3 [Hz]		df_3/f_3
		H	D	[%]	H	D	[%]	H	D	[%]
∞	exact	1.51	1.40	7%	4.96	4.62	7%	9.68	9.46	2%
10^{20}	MUSIC	1.56	1.44	8%	4.97	4.67	6%	9.69	9.76	1%
30		1.56	1.43	8%	4.97	4.67	6%	9.68	9.75	1%
10		1.56	1.43	8%	4.96	4.66	6%	9.58	9.74	2%

**H: healthy; D: damaged*

Table 5. Assessment of MUSIC spectra from co-prime sampled noisy measurements for damage detection based on structural natural frequency shifts: damage state 2

SNR [dB]	State*	f_1 [Hz]		df_1/f_1	f_2 [Hz]		df_2/f_2	f_3 [Hz]		df_3/f_3
		H	D	[%]	H	D	[%]	H	D	[%]
∞	exact	1.51	1.07	29%	4.96	3.97	20%	9.68	9.09	6%
10^{20}	MUSIC	1.56	1.13	27%	4.97	3.98	20%	9.69	9.38	3%
30		1.56	1.13	28%	4.97	3.98	20%	9.68	9.36	3%
10		1.56	1.13	28%	4.96	3.97	20%	9.58	9.21	4%

**H: healthy; D: damaged*

Gkoktsi K and Giaralis A (2020) A compressive MUSIC spectral approach for identification of closely-spaced structural natural frequencies and post-earthquake damage detection. *Probabilistic Engineering Mechanics*, accepted: 27/12/2019.

5 Concluding Remarks

A novel natural frequency identification and damage detection approach has been established utilizing response acceleration measurements of white-noise excited structures sampled at rates significantly below the Nyquist rate supporting reduced data transmission in wireless sensors for vibration-based structural monitoring. The approach relies on the standard MUSIC pseudo-spectrum applied to the autocorrelation function of response acceleration time-histories estimated from co-prime sampled sub-Nyquist measurements. In this context, acceleration time-histories are treated as realizations of a stationary stochastic process without posing any sparse structure requirements. Further, the considered approach benefits from the super-resolution and denoising capabilities of the MUSIC spectral estimator to achieve high-accuracy in structural natural frequency identification even for noise-corrupted measurements. In this context, the proposed system identification approach relies on estimating the auto-correlation function of stochastic structural response processes directly from noisy co-prime sampled measurements. It was shown that the adopted co-prime MUSIC-based strategy is a potent tool for natural frequency identification within the operational modal analysis context, capable to efficiently address the structural modal coupling effect even by treating response signals buried in noise. This was numerically verified within a simulation-based framework using accelerations responses originating from a white-noise excited structural system with 2 closely-spaced modes of vibration carrying the same amount of energy, and a 3rd less excited vibrating mode under the considered forcing case. Parametric analyses were conducted using noise-corrupted compressed data at five *SNRs* between 0 and 20 dB, by employing four different pairs of co-prime numbers associated with different sub-Nyquist rates and spectral resolutions. It was shown that higher resolution is achieved at stronger signal compression levels (*i.e.*, larger co-prime numbers), which further allows the separation of very closely-spaced structural resonant frequencies (with a percentage difference of roughly 4.5%) from a significantly reduced number of noisy measurements at *SNRs* as low as 5dB.

Further to the above, a novel structural damage detection approach was proposed, based on changes to the structural natural frequencies, before and after a seismic event of low-intensity. These resonant frequencies are extracted from sub-Nyquist sampled acceleration response signals

within an operational modal analysis framework. It is assumed that within this short time interval (*i.e.*, pre- and post- earthquake), the environmental conditions remain the same and thus any (likely to be slight) change to the natural frequencies is caused by the input seismic action to the structure. The effectiveness and applicability of the proposed approach was numerically evaluated using a white-noise excited linear reinforced concrete 3-storey frame in a healthy and two damaged states caused by two ground motions of increased intensity. The damaged models were simulated with locally reduced effective flexural rigidities (*i.e.*, along the plastic hinge zones), computed by non-linear response history analysis and the Takeda hysteretic model. The numerical results demonstrate that the considered approach is capable to detect very small structural damage directly from the compressed measurements even for high noise levels at *SNR*=10dB. It was further shown that any additive broadband noise during data acquisition does not affect the damage detection capabilities of the proposed approach (at least for the noise levels encountered in practical applications) as such kind of noise is filtered out by application of the MUSIC spectral estimator.

The above results suggest that the adopted approach makes a dependable noise-immune structural damage detection technique that can be potentially embedded within arrays of wireless sensors for cost-efficient (in terms of data sampling and wireless transmission rates) vibration-based structural health monitoring.

Acknowledgments

This work has been partly funded by EPSRC in UK, under grant No EP/K023047/1: the second author is indebted to this support. The first author further acknowledges the support of City, University of London through a PhD studentship.

Gkoktsi K and Giaralis A (2020) A compressive MUSIC spectral approach for identification of closely-spaced structural natural frequencies and post-earthquake damage detection. *Probabilistic Engineering Mechanics*, accepted: 27/12/2019.

References

[1] J.M.W. Brownjohn, C.J. Middleton, Procedures for vibration serviceability assessment of high-frequency floors, Engineering Structures, 30 (2008) 1548-1559.

[2] S. Živanović (2012) Benchmark Footbridge for Vibration Serviceability Assessment under Vertical Component of Pedestrian Load. ASCE Journal of Structural Engineering, 138 (10), 1193-1202. doi: 10.1061/(ASCE)ST.1943-541X.0000571.

[3] O.S. Salawu, Detection of structural damage through changes in frequency: a review. Eng. Struct. 19 (1997) 718-723.

[4] Z. Yang, L. Wang, Structural damage detection by changes in natural frequencies, J. Intelligent material systems and structures, 21 (2010) 309-319. DOI: 10.1177/1045389x09350332.

[5] A. Pau, A. Greco, F. Vestroni, Numerical and experimental detection of concentrated damage in a parabolic arch by measured frequency variations. Journal of Vibration and Control 17 (2010) 605-614.

[6] M. De Angelis, A. Giaralis, F. Petrini, D. Pietrosanti (2019) Optimal tuning and assessment of inertial dampers with grounded inerter for vibration control of seismically excited base-isolated systems. *Engineering Structures*, 196: 109250. DOI: 10.1016/j.engstruct.2019.05.091.

[7] P. Cacciola, A. Tombari, A. Giaralis A. An inerter-equipped vibrating barrier for non-invasive seismic protection of existing structures. *Structural Control and Health Monitoring, accepted.*

[8] L. Marian, Giaralis A. (2017). The tuned mass-damper-inerter for harmonic vibrations suppression, attached mass reduction, and energy harvesting. *Smart Structures and Systems*, **19**(6): 665-678.

[9] J.M.W. Brownjohn, E.P. Carden, C.R. Goddard, G. Oudin, Real-time performance monitoring of tuned mass damper system for a 183m reinforced concrete chimney, J. Wind Eng. Ind. Aerodyn. 98 (2010) 169–179.

[10] R. Brincker, C.E. Ventura, Introduction to Operational Modal Analysis, John Wiley & Sons, Ltd, Chichester, UK (2015). doi:10.1002/9781118535141.

Gkoktsi K and Giaralis A (2020) A compressive MUSIC spectral approach for identification of closely-spaced structural natural frequencies and post-earthquake damage detection. *Probabilistic Engineering Mechanics*, accepted: 27/12/2019.

[11] J.P. Lynch, An overview of wireless structural health monitoring for civil structures, Philos. Trans. R. Soc. A Math. Phys. Eng. Sci. 365 (2007) 345–372. doi:10.1098/rsta.2006.1932.

[12] B.F. Spencer, C. Yun, Wireless Sensor Advances and Applications for Civil Infrastructure Monitoring, (2010).

[13] S.M. O'Connor, J.P. Lynch, A.C. Gilbert, Compressed sensing embedded in an operational wireless sensor network to achieve energy efficiency in long-term monitoring applications, Smart Mater. Struct. 23 (2014) 085014. doi:10.1088/0964-1726/23/8/085014.

[14] J.Y.. Park, M.B.. Wakin, A.C.. Gilbert, Modal analysis with compressive measurements, IEEE Trans. Signal Process. 62 (2014) 1655–1670. doi:10.1109/TSP.2014.2302736.

[15] Y. Yang, S. Nagarajaiah, Output-only modal identification by compressed sensing: Non-uniform low-rate random sampling, Mech. Syst. Signal Process. 56–57 (2015) 15–34. doi:10.1016/j.ymssp.2014.10.015.

[16] Y. Huang, J.L. Beck, S.Wu, H Li, Bayesian compressive sensing for approximately sparse signals and application to structural health monitoring signals for data loss recovery, Probabilistic Engineering Mechanics, 46 (2016), 62-79.

[17] L. Comerford, I.A. Kougioumtzoglou, M. Beer, Compressive sensing based stochastic process power spectrum estimation subject to missing data, Probabilistic Engineering Mechanics 44, 66-76, 2016.

[18] L. Comerford, H.A. Jensen, F. Mayorga, M. Beer, I.A. Kougioumtzoglou, Compressive sensing with an adaptive wavelet basis for structural system response and reliability analysis under missing data. Computers & Structures 182 (2017): 26-40.

[19] R. Klis, E.N. Chatzi, Vibration monitoring via spectro-temporal compressive sensing for wireless sensor networks, Struct. Infrastruct. Eng. 13 (2017) 195–209. doi:10.1080/15732479.2016.1198395.

[20] K. Gkoktsi, A. Giaralis, Assessment of sub-Nyquist deterministic and random data sampling techniques for operational modal analysis, Struct. Heal. Monit. 16 (2017) 630–646. doi:10.1177/1475921717725029.

Gkoktsi K and Giaralis A (2020) A compressive MUSIC spectral approach for identification of closely-spaced structural natural frequencies and post-earthquake damage detection. *Probabilistic Engineering Mechanics*, accepted: 27/12/2019.

[21] K. Gkoktsi, A. Giaralis, A multi-sensor sub-Nyquist power spectrum blind sampling approach for low-power wireless sensors in operational modal analysis applications, Mech. Syst. Signal Process. 116 (2019) 879–899. doi:10.1016/j.ymssp.2018.06.049.

[22] K. Gkoktsi, A. Giaralis, R.P. Klis, V. Dertimanis, E.N. Chatzi. Output-only vibration-based monitoring of civil infrastructure via sub-Nyquist/compressive measurements supporting reduced wireless data transmission, *Frontiers in Built Environment: Structural Sensing, accepted.*

[23] R. Baraniuk, Compressive Sensing [Lecture Notes]. *IEEE Signal Process Mag* 2007; 24(4): 118–121.

[24] P.P. Vaidyanathan, P. Pal, Sparse Sensing With Co-Prime Samplers and Arrays, IEEE Trans. Signal Process. 59 (2011) 573–586. doi:10.1109/TSP.2010.2089682.

[25] S.L. Marple, Digital spectral analysis, Prentice-Hall, Englewood Cliffs, 1987.

[26] P. Pal, P.P Vaidyanathan, Nested arrays: a novel approach to array processing with enhanced degrees of freedom. IEEE Trans. Signal Process. 58 (2010) 4167–4181.

[27] D. Camarena-Martinez, J.P. Amezquita-sanchez, M. Valtierra-rodriguez, R.J. Romero-troncoso, R.A. Osornio-rios, A. Garcia-perez, EEMD-MUSIC-Based Analysis for Natural Frequencies Excitations, Sci. World J. 2014 (2014) 1–12.

[28] J.P. Amezquita-Sanchez, A. Garcia-Perez, R.J. Romero-Troncoso, R.A. Osornio-Rios, G. Herrera-Ruiz, High-resolution spectral-analysis for identifying the natural modes of a truss-type structure by means of vibrations, J. Vib. Control. 19 (2012) 2347–2356. doi:10.1177/1077546312456228.

[29] Jiang, X. & Adeli, H., Pseudospectra, MUSIC, and dynamic wavelet neural network for damage detection of highrise buildings. International Journal for Numerical Methods in Engineering, 71(5), (2007), 606–629.

[30] Rainieri, C., Fabbrocino, G., Manfredi, G. & Dolce, M., Robust output-only modal identification and monitoring of buildings in the presence of dynamic interactions for rapid post-earthquake emergency management. *Engineering Structures*, 34, (2012), 436–446.

Gkoktsi K and Giaralis A (2020) A compressive MUSIC spectral approach for identification of closely-spaced structural natural frequencies and post-earthquake damage detection. *Probabilistic Engineering Mechanics*, accepted: 27/12/2019.

[31] Foti, D., Gattulli, V. & Potenza, F., Output-Only Identification and Model Updating by Dynamic Testing in Unfavorable Conditions of a Seismically Damaged Building. *Computer-Aided Civil and Infrastructure Engineering*, 29(9), (2014), 659–675.

[32] B. Decarli, A. Giaralis, Modal strain-based post-earthquake damage characterization of r/c frame buildings, 16th European Conference on Earthquake Engineering, paper #11208, pp 10.

[33] M. Shinozuka, G. Deodatis, Simulation of stochastic processes by spectral representation. Appl. Mech. Rev. 44 (1991): 191-204.

[34] K. Gkoktsi, A. Giaralis, Effect of frequency domain attributes of wavelet analysis filter banks for structural damage localization using the relative wavelet entropy index. International Journal of Sustainable Materials and Structural Systems, 2 (2015) 134–160.

[35] Ewins, D.J., Modal testing: Theory practice and application, 2nd ed., Research Studies Press. Baldock (2000).

[36] T.T. Soong, M. Grigoriu, Random Vibration of Mechanical and Structural Systems, Prentice Hall PTR, 1996.

[37] P.D. Spanos, B.A. Zeldin, Monte Carlo Treatment of Random Fields: A Broad Perspective, Appl. Mech. Rev. 51 (1998) 219–237. doi:10.1115/1.3098999.

[38] A. Giaralis, P.D. Spanos, Wavelet-based response spectrum compatible synthesis of accelerograms—Eurocode application (EC8), Soil Dyn. Earthq. Eng. 29 (2009) 219–235. doi:10.1016/j.soildyn.2007.12.002.

[39] A. Giaralis, P.D. Spanos, Derivation of response spectrum compatible non-stationary stochastic processes relying on Monte Carlo-based peak factor estimation, Earthquakes Struct. 3 (2012) 581–609. doi:10.12989/eas.2012.3.5.719.

[40] Gattulli V, Potenza F, Graziosi F, Federici F, Colarieti A, Faccio M (2014): Distributed Structural Monitoring for a Smart City in a Seismic Area. Key Engineering Materials, 628: 123–135.

[41] Priestley MJN, Calvi GM, Kowalsky MJ (2007): *Displacement-based seismic design of structures*. IUSS Press.

Gkoktsi K and Giaralis A (2020) A compressive MUSIC spectral approach for identification of closely-spaced structural natural frequencies and post-earthquake damage detection. *Probabilistic Engineering Mechanics*, accepted: 27/12/2019.

[42] Takeda, Sozen, Nielsen (1970): Reinforced Concrete Response to Simulated Earthquakes. *Journal of the Structural Division*, **96** (12), 2557–2573.

[43] I. Avramidis, A. Athanatopoulou, K. Morfidis, A. Sextos, and A. Giaralis, Eurocode-Compliant Seismic Analysis and Design of R/C Buildings Concepts, Commentary and Worked Examples with Flowcharts. Cham: Springer International Publishing, 2016.